In the energetically best crystal structure the Br atoms form a distorted cubic close packing, with the Si atoms occupying 1/8 of the tetrahedral voids in such a way that the molecules themselves also form a distorted cubic close packing. This structure type is found experimentally for CF_4 and $PbCl_4$. In the other low-energy structures the Br atoms adopt various sphere packings.

[1] *Schaloske, M.C., L. Kienle, C. Hoch, Hj. Mattausch, R.K. Kremer and A. Simon.* Zeitschrift für anorganische und allgemeine Chemie **635**, 1023–1029 (2009).

[2] *Schaloske, M.C., Hj. Mattausch, L. Kienle and A. Simon.* Zeitschrift für anorganische und allgemeine Chemie **634**, 1493–1500 (2008).

[3] *Babizhetskyy, V., Hj. Mattausch and A. Simon.* Zeitschrift für Naturforschung B **63**, 929–933 (2008).

[4] *Hoch, C. and A. Simon.* XIIth European Conference on Solid State Chemistry, Münster, 166 (2009).

[5] *Hoch, C., J. Bender and A. Simon.* Angewandte Chemie International Edition **48**, 2415–2417 (2009).

[6] *Hoch, C., J. Bender, A. Wohlfarth and A. Simon.* Zeitschrift für anorganische und allgemeine Chemie **635**, 1777–1782 (2009).

[7] *Wolf, A.K., J. Glinnemann, M.U. Schmidt, J. Tong, R.E. Dinnebier, A. Simon and J. Köhler.* Acta Crystallographica B **65**, 342–349 (2009).

Chain manganates: A new family of mixed-valent one-dimensional transition metallates

J. Nuss, M. Stahl, S. Pfeiffer, M.A. Señarís-Rodríguez and M. Jansen

Charge, spin and orbital ordering are regarded as crucial prerequisites for the occurrence of collective physical phenomena like high-T_c superconductivity or pronounced magnetoresistance in extended solids showing low-dimensional substructures. In most instances the required mixed-valence state of the respective transition metal has been introduced by extrinsic doping. Such an approach, however, has the unfavorable side effect of broken translational symmetry (perturbed periodicity).

Recently, we have developed the azide/nitrate route for the synthesis of alkali oxometallates. It allows for a remarkably minute control and adjustment of the compositions, including the oxygen contents, of the targeted transition metallates, opening a versatile access to intrinsically doped extended oxides [1]. Among the transition elements manganese stands out, because of its richness in accessible oxidation states, and thus appears to be particularly suitable for further probing the potential of the azide/nitrate route. By increasing the alkali metal to manganese ratio beyond the values typical for, e.g., hollandites like $Rb_{1-x}Mn_4O_8$, we have been able to shift the oxidation state of manganese to lower values (2+/3+) and to break down the three-dimensional framework of the anionic MnO_2 part of the hollandite to a one-dimensional partial structure, with an amazingly ample family of intrinsically doped new oxomanganates emerging.

The compositions realized thus far,

- $K_{29}Mn_{17}O_{34}$ [2],
- $Rb_{11}Mn_8O_{16}$ [2,3],
- $Rb_{15}Mn_{11}O_{22}$ [3,4],
- $Cs_4Mn_3O_6$ [2], and
- $Cs_{23}Mn_{16}Mn_{28}$,

were obtained from stoichiometric mixtures of the precursors Mn_2O_3, ANO_3 and AN_3 (A = K, Rb, Cs) in steel containers, provided with silver inlays. Equation (1) gives the ratio required for $Rb_{11}Mn_8Mn_{16}$, as an example.

$$58\,RbN_3 + 8\,RbNO_3 + 24\,Mn_2O_3 \longrightarrow 6\,Rb_{11}Mn_8O_{16} + 91\,N_2 \quad (1)$$

With the exception of $Cs_{23}Mn_{16}O_{28}$, the compositions can be generalized as A_xMnO_2 with x varying from 1.706 to 1.333. The most prominent structural feature, shared by all of the A_xMnO_2 compounds, is a one-dimensional polyanion $^1_\infty[MnO_2]^{n-}$ constituted of edge sharing, sometimes heavily distorted, MnO_4 tetrahedra, forming a hexagonal rod-packing. The alkali metal ions fill the space between the anionic entities resulting in a honeycomb like topology. Figure 8 shows the structural principle (for example of $Rb_{15}Mn_{11}O_{22}$).

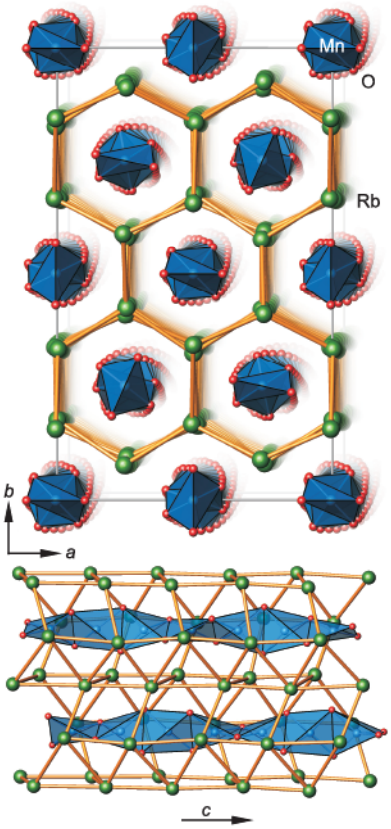

Figure 8: Above: perspective representation of the crystal structure of $Rb_{15}Mn_{11}O_{22}$, with margins of the unit cell (grey); shortest Rb–Rb contacts are drawn by orange sticks. Below: Structural fragment, showing two of the $^1_\infty[MnO_2]^{n-}$ chains of edge chairing MnO_4 tetrahedra in c-direction.

Obviously manganese is in a mixed-valent state. One may assign average or split valences, corresponding to

$K_{29}Mn^{II}_{12}Mn^{III}_5O_{34}$ or $K_{28}Mn^{+2.294}_{17}O_{34}$,
$Rb_{11}Mn^{II}_3Mn^{III}_5O_{16}$ or $Rb_{11}Mn^{+2.625}_8O_{16}$,
$Rb_{15}Mn^{II}_4Mn^{III}_7O_{22}$ or $Rb_{15}Mn^{+2.636}_{11}O_{22}$, and
$Cs_4Mn^{II}Mn^{III}_2O_4$ or $Cs_4Mn^{+2.667}_3O_6$.

Fully ordered charges should be reflected by specific Mn–O distances. For a tetrahedral coordination one would expect Mn–O bond lengths of 1.9 Å (Mn^{3+}) and 2.0 Å (Mn^{2+}), respectively. Upon inspecting the interatomic distances found experimentally, one notices significant spreads from 1.84 Å to 2.11 Å, covering the full range expected for the distances of Mn^{3+} and Mn^{2+} to oxygen.

Another significant structural detail results from the necessity to adjust the translation period of the MnO_2 chains to the alkali metal framework. For $Cs_4Mn_3O_6$ a simple formula for the average compatible periodicities can be given: $3\times d_{Mn-Mn} = 2\times d_{Cs-Cs} = c = 8.179(2)$ Å. Finding the smallest common denominator for the other representatives leads to extraordinarily long crystallographic axes:

$K_{29}Mn_{17}O_{34}$
$[34\times d_{Mn-Mn} = 29\times d_{K-K} = a = 93.149(3)$Å$]$,
$Rb_{11}Mn_8O_{16}$
$[16\times d_{Mn-Mn} = 11\times d_{Rb-Rb} = c = 43.712(2)$ Å$]$
and $Rb_{15}Mn_{11}O_{22}$
$[22\times d_{Mn-Mn} = 15\times d_{Rb-Rb} = c = 59.798(2)$ Å$]$.

As a consequence of this matching of the translation vectors of the $^1_\infty MnO^{n-}_2$ polyanions and the respective alkali ions, the oxidation state of manganese is fixed. The smaller cation generates a larger ratio between alkali metal and manganese in $K_{29}Mn_{17}O_{34} = K_{1.706}MnO_2$, and consequently a larger ratio of $Mn^{2+}/Mn^{3+} = 0.71/0.29$. The bigger cesium ion only allows for a smaller ratio Cs/Mn ($Cs_4Mn_3O_6 = Cs_{1.333}MnO_2$), and thus a smaller ratio $Mn^{2+}/Mn^{3+} = 0.33/0.67$ results. Finally, the oxygen atoms, which form a screw around the manganese backbone, have to match the coordinative requirements of both, the alkali metals and the manganese atoms (Fig. 8).

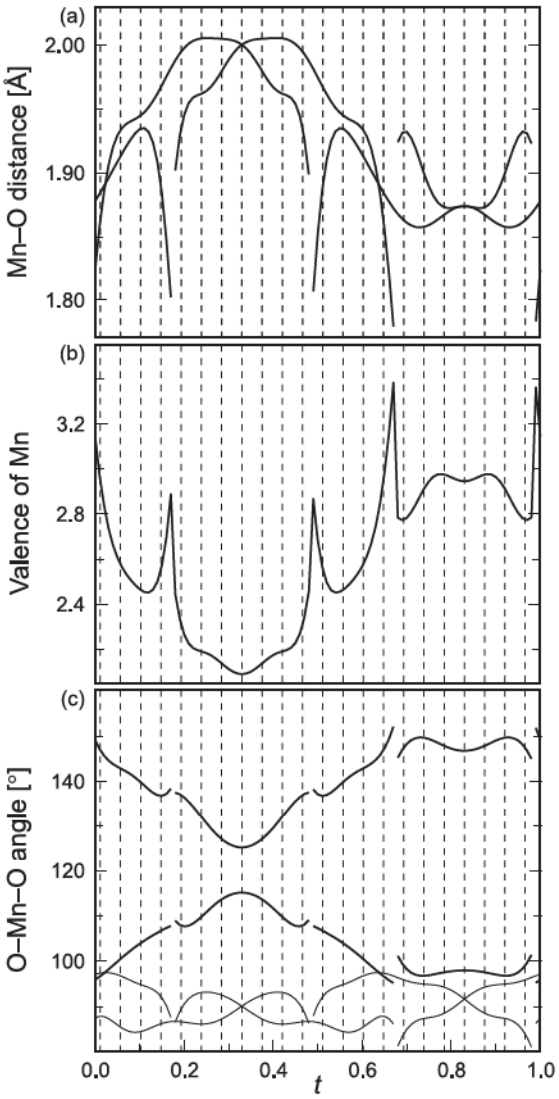

Figure 9: Coordination of Mn in $Rb_{15}Mn_{11}O_{22}$: (a) *t*-plot (modulation function [5]) of the four Mn–O distances of the first coordination shell. (b) *t*-plot of the valence of Mn obtained by the bond-valence method. (c) the six O–Mn–O angles as a function of the parameter *t*. (a)–(c) vertical dashed lines indicate those values of *t* that are realized in the commensurate composite structure; bold lines have to be counted twice due to symmetry relations.

The modulations of the charges of manganese, and the periodicity of the alkali metal framework diverging from the one of the MnO_2 chains can be more appropriately addressed within the (3+1)D superspace approach [5]. At least $Rb_{11}Mn_8O_{16}$ and $Rb_{15}Mn_{11}O_{22}$ can be described as composite structures consisting of two subcells, one for the rubidium and another for the MnO_2 substructures, whereby the intersubsystem contacts result in a displacive modulation, mainly of the oxygen atoms [3]. A uniform and inclusive description is provided by analyzing the modulation function (*t*-plots Fig. 9): The Mn–O bond has not only one optimal value, but the modulation of the coordination of Mn reflects the two limiting valence states of this atom. This results in Mn–O bonds being longer for Mn^{2+} than for Mn^{3+}, on the average (Fig. 9(a), the four Mn–O bonds are pairwise equal). The relatively large variation of Mn–O bond length from 1.80 Å to 2.05 Å can indeed be explained by the two valence states of Mn as it is shown by the valence sums computed by the bond-valence method (Fig. 9(b)). The helical MnO_2 chains are composed of strongly distorted $MnO_{4/2}$ tetrahedra. Each two O–Mn–O angles that are related to the two edges connecting two polyhedra are in the range of 90° (thin lines in Fig. 9(c)) and show smaller variations as compared to the remaining four angles. The latter can be divided into two subsets, with angles around 105° and around 135°, respectively (bold lines, Fig. 9(c)).

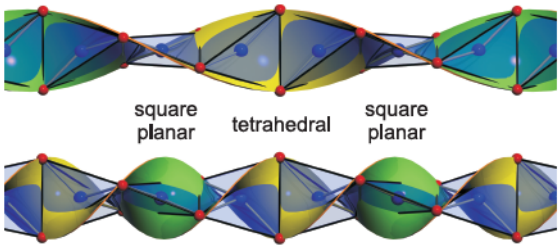

Figure 10: Fragment of the crystal structure of $Rb_{15}Mn_{11}O_{22}$ with right-handed (top) and left-handed (below) helicoidally surface, emphasizing the helicoidally shaped MnO_2 chain with alternating, more like tetrahedral and square planar coordination of manganese.

The extreme values of ≈95° and ≈150° are indicative for an approximately square planar configuration (ideal angles 90° and 180°), while those of ≈115° and ≈125° are approaching the value expected for a tetrahedron (ideal angles 109°, each). Taking the information contained in Figs. 9(a)–(c), together, confirms that

the surrounding of Mn^{2+} is a distorted tetrahedron and the one of Mn^{3+} approaches a square planar-like coordination, respectively. Although the modulations of distances and angles indicate an intermediate valence state of Mn, a value of $\approx 1/2$ can be roughly estimated for the tetrahedral/planar and thus the Mn^{2+}/Mn^{3+} ratio (Fig. 10). This ratio is in agreement with the mixed-valence character of manganese as it can be deduced from the compositions of both compounds $Rb_{11}Mn_8O_{16}$ and $Rb_{15}Mn_{11}O_{22}$, with $Mn^{2+}/Mn^{3+} \approx 1/2$.

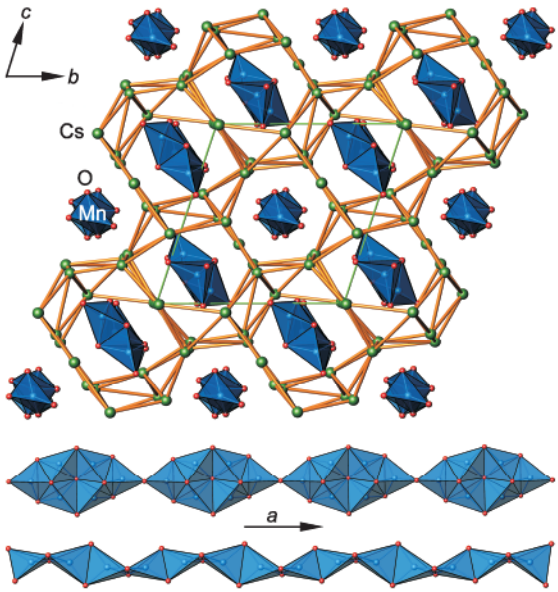

Figure 11: Above: Representation of the crystal structure of $Cs_{23}Mn_{16}O_{28}$, with margins of the unit cell (green); shortest Cs–Cs contacts are drawn by orange sticks. Below: $^1_\infty[MnO_2]^{n-}$ and $^1_\infty[Mn_3O_5]^{m-}$ chains of edge and corner chairing MnO_4 tetrahedra in *a*-direction.

Turning to the exception mentioned in the beginning, the compound $Cs_{23}Mn^{II}_{15}Mn^{III}O_{28}$, it is obvious from the overall composition that only one out of the 16 manganese atoms is trivalent and that the anionic partial structure can no longer consist of $^1_\infty MnO_2^{n-}$ chains exclusively. Indeed, a new one-dimensional polyanion is present, with the building motif being clusters of six MnO_4 tetrahedra, each linked by common edges. Such clusters are finally connected by sharing oxygen atoms (common corners) forming $^1_\infty Mn_3O_5^{m-}$ chains (Fig. 11).

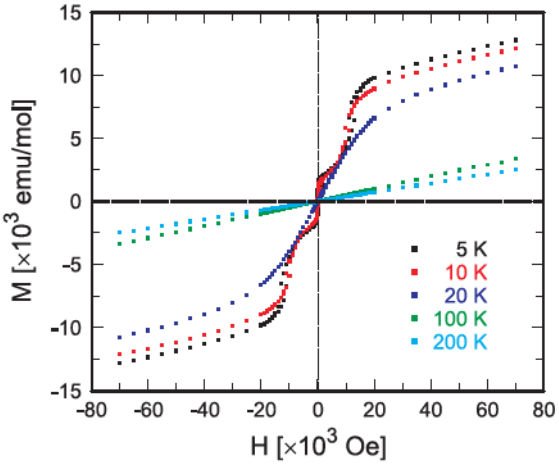

Figure 12: Field-dependent measurement of the magnetization of $Cs_{23}Mn_{16}O_{28}$ at different temperatures.

Since each member of the novel family of intrinsically doped manganates displays a distinct spontaneous electric and magnetic polarization, and, coupled to the latter, also an elastic deformation, this class of compounds appears to be a promising system for comparative studies on multiferroic properties, as well as on charge, spin and orbital ordering. Figure 12 demonstrates the spontaneous magnetization and the occurrence of different magnetic states for $Cs_{23}Mn_{16}O_{28}$.

In Collaboration with:
S. van Smaalen (Universität Bayreuth)

[1] *Trinschek, D. and M. Jansen.* Angewandte Chemie International Edition **38**, 133–135 (1999).

[2] *Pfeiffer, S., J. Nuss and M. Jansen.* Zeitschrift für anorganische und allgemeine Chemie **636**, 23–29 (2010).

[3] *Nuss, J., S. Pfeiffer, S. van Smaalen and M. Jansen.* Acta Crystallographica B **66**, 27–33 (2010).

[4] *Pfeiffer, S., J. Nuss and M. Jansen.* Zeitschrift für Kristallographie: New Crystal Structures **224**, 377–378 (2009).

[5] *van Smaalen, S.* Zeitschrift für Kristallographie **219**, 681–691 (2004).